Available online at www.sciencedirect.com
ScienceDirect
Acta Materialia 59 (2011) 4999–5011
Acta MATERIALIA
www.elsevier.com/locate/actamat

Martensite aging effects on the dynamic properties of Au–Cd shape memory alloys: Characteristics and modeling

Dezhen Xue [a,b,*], Yumei Zhou [a,b], Xiangdong Ding [a], Kazuhiro Otsuka [b], Jun Sun [a], Xiaobing Ren [a,b]

[a] Multi-Disciplinary Materials Research Center, Frontier Institute of Science and Technology, State Key Laboratory for Mechanical Behavior of Materials, Xi'an Jiaotong University, Xi'an 710049, People's Republic of China
[b] Ferroic Physics Group, National Institute for Materials Science, Tsukuba, 305-0047 Ibaraki, Japan

Received 20 January 2011; received in revised form 17 April 2011; accepted 20 April 2011
Available online 26 May 2011

Abstract

We revisit the martensite aging effect in Au–Cd alloys, by studying the evolution of dynamic properties (i.e. storage modulus and internal friction) with aging time. We found that the storage modulus shows a gradual increase while the internal friction shows a gradual decrease with increasing aging time. Moreover, the evolution of dynamic properties with aging time obeys a simple relaxation function with activation energy of 0.46 eV in $AuCd_{49.5}$ alloy. The dependence of such evolution on temperature, defect concentration, frequency and displacement amplitude was also well characterized. All the observed characteristics are understood by the gradual stabilization of martensite phase during aging, driven by a symmetry-conforming short-range ordering tendency of point defects. Furthermore, we proposed a homogenous Landau-type model to describe the response of storage modulus during aging by introducing a time-dependent variable coupled with the order parameter. Such systematic investigation on the dynamic properties during martensite aging is crucial for applications under mechanical vibrations.
© 2011 Acta Materialia Inc. Published by Elsevier Ltd. All rights reserved.

Keywords: Martensite; Aging; Shape memory alloy; Storage modulus; Internal friction

1. Introduction

Shape memory alloys (SMAs) are of considerable interest for their technological applications, ranging from actuators to sensors [1]. With decreasing temperature, they undergo a symmetry-lowering transformation from the high-symmetry parent phase to the low-symmetry martensite phase [2]. However, in the martensite phase, a majority of SMAs, such as Au–Cd [3,4], Au–Cu–Zn [5], Cu–Zn–Al [6,7], Cu–Al–Ni [8], Ti–Ni–Hf [9] and Ni–Mn–Ga [10], exhibit martensite aging effects, i.e. a gradual change of physical properties with aging time. As the martensite aging effects, in general, are undesirable for applications of shape memory alloys [1,11], the problem has attracted much attention, not only in probing its time-dependent characteristics but also in pursuing its physical origin.

The martensite aging effects on the static properties of SMAs have been studied to a great degree in past decades, particularly the after-effect of martensite aging, i.e. the change of static properties after martensite aging. On the one hand, quite rich experimental phenomena were revealed by past studies. The most striking martensite aging effects involve two aspects. One is the rubber-like behavior (RLB), that is, the martensitic alloy after being aged for some time in the martensite phase exhibits recoverable or pseudo-elastic deformation behavior [3,5,8,12]. The other is the martensite stabilization effect, i.e. the martensite phase becomes more stable after aging, which is manifested by the fact that the finishing temperature of

* Corresponding author. Tel.: +86 02983395126; fax: +86 02983395131.
E-mail address: Xuedezhen@gmail.com (D. Xue).

1359-6454/$36.00 © 2011 Acta Materialia Inc. Published by Elsevier Ltd. All rights reserved.
doi:10.1016/j.actamat.2011.04.050

reverse martensitic transformation (A_f) increases with increasing aging time [6,9–10]. Up to now, the martensite aging effects on those static properties and how they evolve with aging time have already been experimentally well established [3–10,12–14].

On the other hand, many researchers contributed to the understanding of the origin of the above martensite aging phenomena and several models were proposed, for example the pseudo-twin-type model [15], the long-range ordering model [6], short-range ordering model [7,16], the dislocation model [17], and the domain boundary pinning model [18]. However, these models failed to meet generality criteria, although they were able to explain the martensite aging phenomena to some extent (see Refs. [13,19] for a detailed and critical review for these models of aging). Ren and Otsuka proposed the symmetry-conforming short-range order (SC-SRO) principle, which appears to be able to explain available experimental observations qualitatively and is indirectly evidenced by transmission electron microscopy (TEM) observation and the small change in the symmetry of X-ray diffraction (XRD) profile [12–14]. The main idea of the SC-SRO principle is that the short-range order symmetry of point defects follows the crystal symmetry when in equilibrium [12–14,20]. During martensite aging, the short-range order of point defects with cubic symmetry gradually conforms to the crystal symmetry of martensite phase by reconfiguration of vacancies/anti-site defects [12–14,20]. Several researchers [21–23] have also formulated phenomenological theories to model the RLB and the martensite stabilization, by considering the contribution of SC-SRO tendency of point defects to the Landau–Ginzburg free energy. Recent Monte Carlo and molecular dynamics simulations have also probed the change of short-range order parameters during martensite aging process at atomic level [24].

Despite these extensive studies of martensite aging effects on the static properties, the SMA-based devices are inevitably under certain dynamic load in applications [1,25–28], during which martensite aging could take place as well. Thus, study of martensite aging effects on the corresponding dynamic properties is crucial to applications under mechanical vibrations. Different from studies on the static properties, it mainly refers to probing the in situ change of dynamic properties during the aging process. Researchers have seldom considered such aging aspects, although Nakanishi et al. showed the change of internal friction of $AuCd_{47.5}$ alloy with aging time, which was measured by the composite piezoelectric oscillator method with a frequency of 70 kHz; Murakami et al. briefly showed the change of internal friction and dynamic Young's modulus of $AuCd_{49.5}$ alloy during martensite aging, which was done by the free decay method by using the thin-foiled specimen [18,29]. Nevertheless, systematic investigation of this important issue has not been carried out until now. Furthermore, phenomenological modeling on the change of dynamic properties during martensite aging process also remains covered. Thus, one target of our present work is to probe the in situ change of dynamic properties (storage modulus and internal friction) during martensite aging by dynamic mechanical experiment. The other target is to establish a corresponding phenomenological model for the experimental results. As the internal friction is rather complex, only modeling on the change of storage modulus with aging time has been considered here.

Therefore, in this study, on one hand, we performed systematic experiments on Au–Cd shape memory alloys to study how the dynamic properties, i.e. storage modulus and internal friction, evolve with aging time. It is found that martensite aging results in a gradual increase of storage modulus and a gradual decrease of internal friction. The influences of temperature, defect concentration, frequency, and displacement amplitude on the change of dynamic properties were also systematically characterized. We suggest that the evolution of dynamic properties can be ascribed to the gradual stabilization of martensite phase during aging, driven by a symmetry-conforming short-range ordering tendency of point defects. On the other hand, by introducing a time-dependent variable coupled with the order parameter, a homogenous Landau-type model was proposed to simply describe how the free energy landscape varies with martensite aging. As the second derivative of free energy is the storage modulus, we can obtain the evolution of storage modulus with aging time consequently, which shows good agreement with our experimental observations.

2. Experimental procedures

In the present study, the Au–Cd alloys ($AuCd_{49.5}$ and $AuCd_{50.0}$) were employed. Base ingots were made by melting 99.99% pure Au and 99.99% pure Cd in a sealed quartz tube with Ar gas at 1273 K. The ingots were again melted at 1003 K under the same condition for shaping. The weight of alloys was measured before and after the melting to confirm that the weight loss is negligible. After homogenization at 803 K for 24 h in Ar atmosphere, specimens were spark-cut into proper sizes for each measurement. They were solution-treated at 803 K for 1 h in Ar atmosphere followed by furnace-cooling or quenching into ice-water. Differential scanning calorimetry (DSC) measurement is done to characterize the martensitic transformation temperature of Au–Cd alloys, with a cooling and heating rate of 5 K min^{-1}.

The martensite aging effects on the dynamic properties (storage modulus and internal friction ($\tan\delta$)) were measured by dynamical mechanical analysis (DMA) measurement in a single cantilever mode. During DMA measurement, the specimen was cooled to the aging temperature with cooling rate of 2 K min^{-1} and then aged at this temperature. When the temperature of the specimen is stable, the dynamic properties as a function of aging time were recorded. In order to erase the influence of martensite aging effect at one testing temperature on the results of the next

testing temperature, we heated the specimen to high temperature, 423 K (far above A_f temperature) and maintained it for 30 min to erase the martensite aging effect for each testing run. Furnace-cooled $AuCd_{49.5}$ alloy was aged at different temperatures (258, 263, 268, 273, 278, 283, 288, 293, 298 K), different displacement amplitudes (5, 10, 15, 20, 30 μm, the corresponding strain amplitudes are 0.57, 1.13, 1.70, 2.26, 3.6×10^{-3}) different frequencies (0.2, 0.4, 1, 4, 10, 20 Hz) to investigate the temperature, displacement amplitude and frequency dependence of dynamic properties during aging. Besides furnace-cooled $AuCd_{49.5}$ alloy, furnace-cooled and water-quenched $AuCd_{50.0}$ alloys were also aged at the above different temperatures to study the defect concentration dependence of the evolution of dynamic properties during aging.

3. Experimental results

3.1. Martensitic transformation behavior characterized by the dynamic mechanical properties for furnace-cooled $AuCd_{49.5}$ alloy

As is known, the furnace-cooled $AuCd_{49.5}$ alloy undergoes a β_2 (B2) to ζ_2' (trigonal) martensitic transformation. Fig. 1a and b shows the storage modulus and internal friction vs. temperature curves upon cooling and heating under various frequencies for this specimen. It can be seen that the β_2 to ζ_2' martensitic transformation is characterized by a frequency-independent sharp storage modulus dip and a sharp internal friction peak, which result from the elastic softening and the hysteretic movement of both parent–martensite phase boundaries and twin boundaries under the ac external stress field during DMA measurement, respectively. The martensitic transformation temperature (M_s) is about 303 K, which shows agreement with the DSC result (Fig. 1c). Then the martensite aging experiments were done at temperatures at least 5 K below the M_s, as described in Section 2.

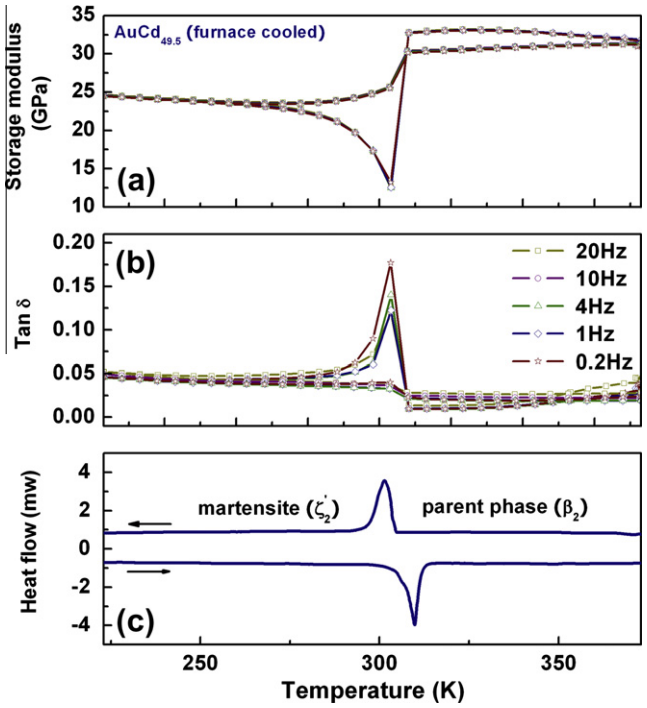

Fig. 1. Martensitic transformation in furnace-cooled $AuCd_{49.5}$ alloy characterized by (a) storage modulus, (b) internal friction by dynamic mechanical analysis (DMA) measurement, and (c) heat flow by differential scanning calorimetry (DSC) measurement.

3.2. Evolution of storage modulus and internal friction as a function of aging time for furnace-cooled $AuCd_{49.5}$ alloy

In the following, we will show how the dynamic properties evolve during martensite aging for the furnace-cooled $AuCd_{49.5}$ specimen. Fig. 2 shows storage modulus (Fig. 2a) and internal friction (Fig. 2b) when the specimen was cooled to 258 K, 268 K, 278 K, 288 K and then held (aged) at these temperatures for 6 h respectively. It is clear that the storage modulus and internal friction indeed vary during martensitic aging. For example, when aged at 288 K, the storage modulus exhibits a gradual increase with aging time (inset of Fig. 2a); in the meantime, the internal friction shows a gradual decrease with time (inset of Fig. 2b). Such behavior is consistent with Murakami et al.'s results [29] of the trigonal martensite in $AuCd_{49.5}$ alloy and also similar with Nakanishi et al.'s results [18] of the orthorhombic martensite in $AuCd_{47.5}$ alloy. Thus, despite martensite phase with different crystal structure, the change of dynamic properties during martensite aging seems to follow the similar tendency.

Furthermore, we find that the data can be well fitted by a stretched exponential function, which is usually employed for describing a relaxation process [30–32]:

$$E'(f,t) = \left\{ E'(f,\infty) - \Delta E'(f,t) \exp\left[-\left(\frac{t}{\tau_0} \right)^{\beta} \right] \right\} \tag{1}$$

where $E'(f,\infty)$ is the equilibrium value of storage modulus when the aging time is infinite, $\Delta E'(f,t)$ $(=E'(f,\infty) - E'(f,0))$ is the absolute change of the storage modulus E' during aging, β is the stretching exponent, and τ is the relaxation time of the aging process. The stretching exponent was fixed at $\beta = 0.75$, as all of the results at different temperature/frequency/amplitude could show best fits of Eq. (1) with $\beta = 0.75$.

In the following three parts, we will utilize this stretched exponential function to study the temperature dependence, displacement amplitude dependence, and frequency dependence of martensite aging effects on the dynamic properties in a quantitative way. For good comparison, all data are normalized by the initial values $E'(f,0)$. Thus the stretched exponential function reads\,

$$E'(f,t)/E'(f,0) = \{E'(f,\infty) - \Delta E'(f,t) \exp\left[-\left(\frac{t}{\tau_0} \right)^{\beta} \right] \Big\} \Big/ E'(f,0) \tag{2}$$

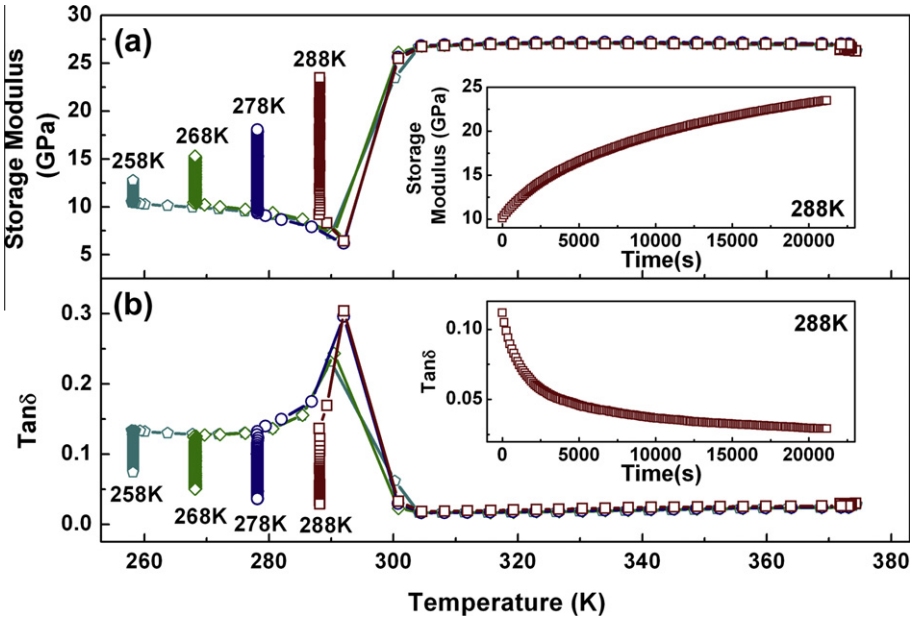

Fig. 2. Storage modulus (a) and internal friction (b) when the furnace-cooled $AuCd_{49.5}$ alloy is cooled down to 288, 278, 268 and 258 K and aged at these temperatures. The inset of (a and b) shows one example showing the evolution of storage modulus and internal friction at 288 K as a function of aging time, respectively.

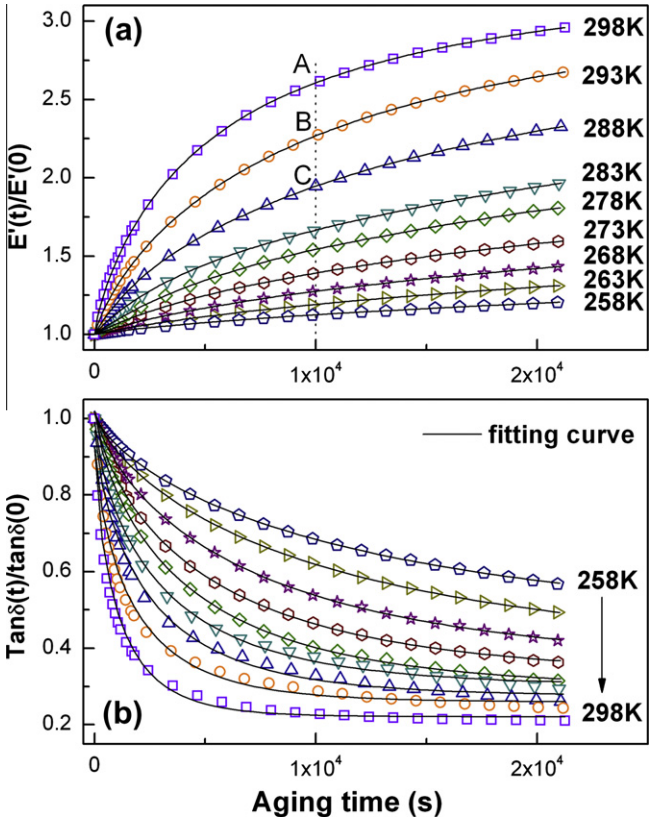

Fig. 3. Dots: evolution of storage modulus (a) and internal friction (b) of the furnace-cooled $AuCd_{49.5}$ alloy at different temperatures from 258 to 298 K; solid line: corresponding fitting curves by the stretched function, $E'(f,t)/E'(f,0) = \left\{E'(f,\infty) - \Delta E'(f,t)\exp\left[-\left(\frac{t}{\tau_0}\right)^{\beta}\right]\right\}\Big/E'(f,0)$.

3.2.1. Temperature dependence

Fig. 3 shows the evolution of storage modulus and internal friction with aging time at different aging temperatures from 258 to 298 K, respectively. It is clear that the martensite aging effects are qualitatively similar for different aging temperatures, i.e. the storage modulus gradually increases with increasing aging time and approaches saturation; the internal friction gradually decreases with aging time and reaches a nearly stable value after long-time aging. However, the change of storage modulus and internal friction exhibit obvious difference for different aging temperature quantitatively. The change of both storage modulus and internal friction increases with increasing aging temperature. For example, at the same aging time 1×10^4 s, the change of storage modulus at 298, 293 and 288 K is indicated by points A, B and C, respectively, as shown in Fig. 3a. In order to explore the microscopic process during aging, we fitted the storage modulus and internal friction vs. aging time curves respectively, by using the above stretched exponential equation (Eq. (2)), as indicated by the solid line in Fig. 3a and b.

Since the obtained parameters after fitting storage modulus and internal friction curves are almost the same, we only show the fitting results of storage modulus here due to space limitation. It can be seen in Fig. 4a that the relaxation time τ increases with decreasing aging temperature, which suggests that the martensite aging process becomes slower with decreasing aging temperature. Furthermore, $\ln(\tau)$ vs. $1/T$ follows the Arrhenius plot and yields an activation energy of 0.46 ± 0.03 eV, which is close to the value obtained through other measurements (0.44 eV) [4]. This indicates that the martensite aging phenomenon is a simple

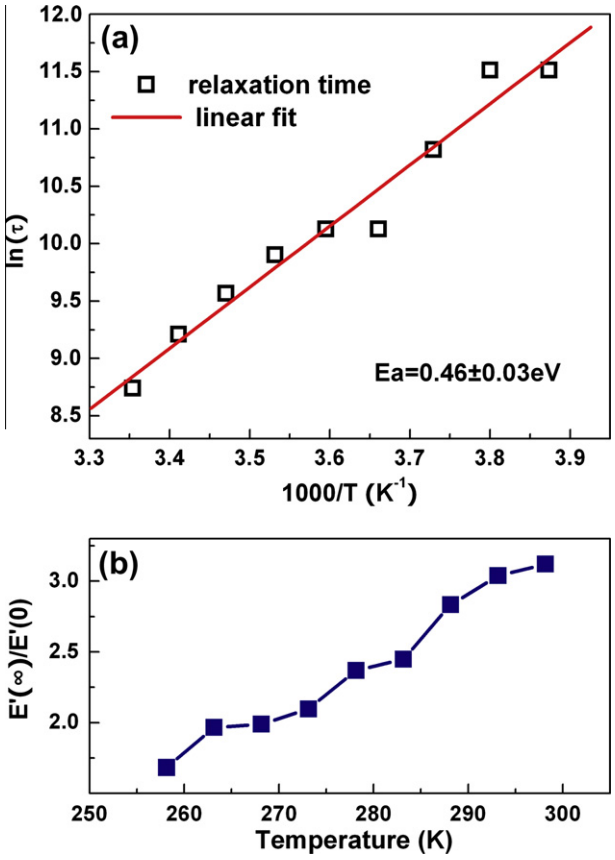

Fig. 4. (a) Relaxation time obtained from fittings in Fig. 3a as a function of the corresponding aging temperature. The linear line is the fitting by Arrhenius relation and the obtained activation energy for the aging process is about 0.46 ± 0.03 eV. (b) The storage modulus at infinite aging time at different aging temperatures got from the fittings in Fig. 3a.

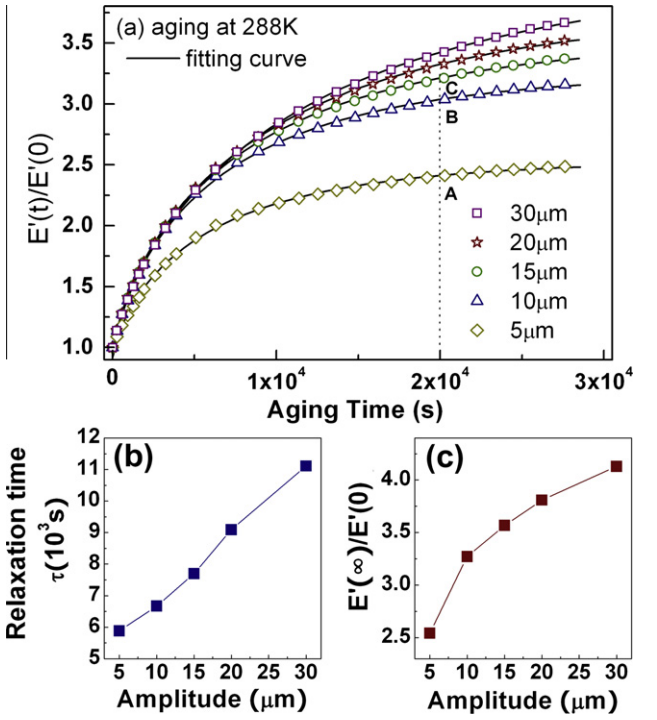

Fig. 5. (a) Dots: evolution of storage modulus when aging at 288 K at different displacement amplitudes during DMA measurement; solid line: corresponding fitting curves by stretched function. (b) The relaxation time at different displacement amplitudes obtained by fittings in (a). (c) Storage modulus at infinite aging time at different displacement amplitudes obtained by fittings in (a).

relaxation process. Fig. 4b shows the normalized storage modulus when the aging time is infinite ($\Delta E'(f,\infty)/E'(f,0)$), and it is clear that it increases with increasing aging temperature.

3.2.2. Displacement amplitude dependence

Here we show only the results for aging at 288 K, since the displacement amplitude dependence is similar for other aging temperatures. The change of storage modulus as a function of aging time for different displacement amplitude is compared in Fig. 5a. For different displacement amplitudes, the storage modulus shows a similar tendency, i.e. it increases with aging time, but the change value of storage modulus shows clear difference for different displacement amplitudes. As shown in Fig. 5a, at the same aging time 2×10^4 s, the change of storage modulus at 5 μm, 10 μm and 15 μm is indicated by points A, B and C respectively, and we can see that it increases with increasing amplitude. These $\Delta E'(f,t)/E'(f,0)$ vs. aging time curves can also be well fitted by Eq. (2). After fitting, the obtained relaxation time τ increases with increasing displacement amplitude, as shown in Fig. 5b. In addition, the normalized storage modulus at infinite aging time ($\Delta E'(f,\infty)/E'(f,0)$) also increases with increasing displacement amplitude, shown in Fig. 5c.

3.2.3. Frequency dependence

Here we show the frequency dependence of martensite aging effects on the dynamic properties. Only the results for aging at 288 K are presented here in Fig. 6a, as the results at other aging temperatures show the similar behavior. It shows that the storage modulus increases with aging time for all the measured frequencies. At short aging time, it seems that the change of storage modulus shows much weaker frequency dependence, compared with its dependence on both temperature and displacement amplitude. At long aging time, the frequency dependence becomes stronger, as indicated by the enlarged part in the inset of Fig. 6a. All these $\Delta E'(f,t)/E'(f,0)$ vs. aging time curves also can be well fitted by Eq. (2). The obtained relaxation time is shown in Fig. 6b and it is clear that the relaxation time decreases with increasing frequency. The obtained change of storage modulus at infinite aging time is shown in Fig. 6c, and it increases with increasing frequency, but the difference between them at different frequencies is very small, for example, the maximum difference between 0.2 and 20 Hz is 2.5%. This could be ascribed to the small frequency range during our measurement, which is limited to low-frequency range.

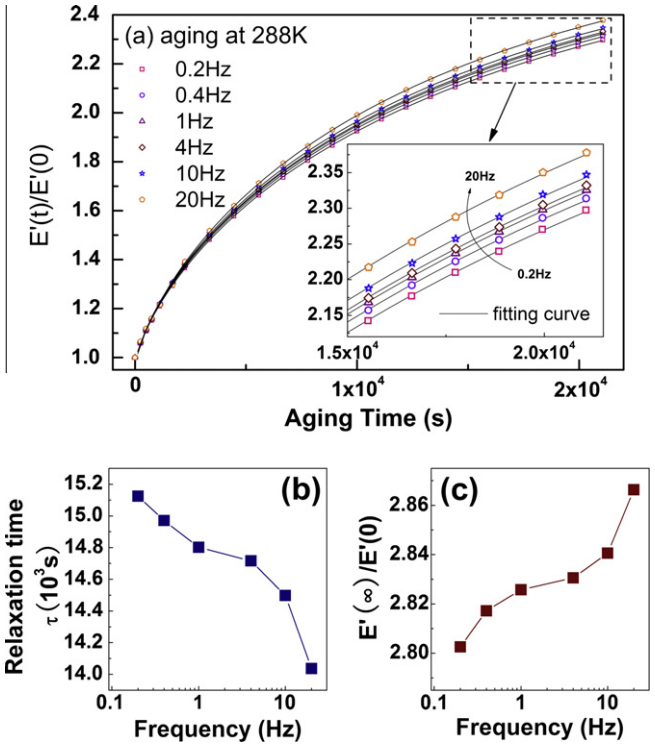

Fig. 6. (a) Dots: evolution of storage modulus when aging at 288 K at different frequencies during DMA measurement; solid line: corresponding fitting curves by stretched function. (b) The relaxation time at different frequencies obtained by fittings in (a). (c) Storage modulus at infinite aging time at different frequencies obtained by fittings in (a).

3.2.4. Heat treatment and defect concentration dependence

The martensite aging effects on the dynamic properties were also investigated for both water-quenched and furnace-cooled stoichiometric $AuCd_{50.0}$ alloys, shown in Fig. 7a1 and a2 and Fig. 7b1 and b2. The martensitic transformation temperatures for these two alloys are 299 K and 300 K respectively by DMA measurement. It is obvious that the evolution of dynamic properties during aging show the similar tendency as that of furnace-cooled $AuCd_{49.5}$ alloy. The storage modulus gradually increases with aging time while the internal friction decreases with aging time. All the $\Delta E'(f, t)/E'(f, 0)$ vs. aging time curves can be well fitted by Eq. (2), as indicated by the solid line in Fig. 7.

In order to compare these three alloys more clearly, we directly put their storage modulus and internal friction vs. aging time curves when aged at the same temperature (293 K) together in Fig. 8a and b, respectively. As can be seen, the change of both storage modulus and internal friction of furnace-cooled $AuCd_{49.5}$ alloy is the most pronounced among these three alloys, the water-quenched $AuCd_{50.0}$ alloy is less pronounced and the furnace-cooled $AuCd_{50.0}$ alloy is the weakest. Fig. 8c shows the Arrhenius relation between relaxation time and aging temperature for these three alloys. The slope represents the activation energy for the aging process in each alloy. The activation energy of water-quenched $AuCd_{50.0}$ alloy is about 0.84 eV, which is the largest among three alloys; and that for furnace-cooled $AuCd_{50.0}$ and furnace-cooled $AuCd_{49.5}$ alloys are 0.49 and 0.46 eV respectively, which are very similar. Such contrasting results seem to suggest that the martensite aging effect on dynamic properties is largely affected by both the type and concentration of point defects in martensitic alloys.

We first compare the furnace-cooled and water-quenched $AuCd_{50.0}$ alloys. As the order–disorder or order–order transition does not occur until right below the melting point for a near-stoichiometric Au–Cd alloy, the vacancy concentration is considered to be the main factor that is sensitive to the heat treatment. As both of them are stoichiometric alloys, there exist few anti-site point defects. Thus vacancies mainly contribute to the aging effect in the two kinds of $AuCd_{50.0}$ alloys. However, the vacancy concentration in the water-quenched $AuCd_{50.0}$ alloy is much higher than that in the furnace-cooled $AuCd_{50.0}$ alloy, so the stronger martensite aging effects in the former one is considered to originate from its higher vacancy concentration. There is a deviation of activation energies for furnace-cooled and water-quenched $AuCd_{50.0}$ alloys. This result is thought to originate from the quenching-induced variables such as vacancy multiplets and changes in order, which complicate the diffusion process of the water-quenched $AuCd_{50.0}$ alloy [33]. For the furnace-cooled $AuCd_{49.5}$ alloy, there are two types of structural defects (anti-site defects and vacancies) and the concentration is highest due to its off-stoichiometry, which could be responsible for the most pronounced martensite aging effects. The above comparison indicates that there indeed exists a close relationship between the change of dynamic properties during aging and the defect concentration. This is similar to the defect concentration dependence of the change of static properties (e.g. critical stress for rearrangement of martensite variants) after martensite aging [4].

In summary, we systematically investigated the in situ evolution of dynamic properties (storage modulus and internal friction) during martensite aging. Our results show that the storage modulus gradually increases with aging time, while the internal friction gradually decreases with aging time. Moreover, we showed that such evolution is strongly dependent on the point defect concentration of the martensitic alloy and the aging temperature, displacement amplitude and frequency, during dynamic loading.

4. Discussions

4.1. Understanding of the evolution of dynamic properties during martensite aging

4.1.1. Gradual martensite stabilization during aging

The above detailed studies describe how the dynamic properties evolve during martensite aging under ac stress field. Now the central question is how to understand such phenomena. As mentioned in the Introduction, the martensite aging effects on the static properties can be understood by the SC-SRO principle [12–14,20]; here it is

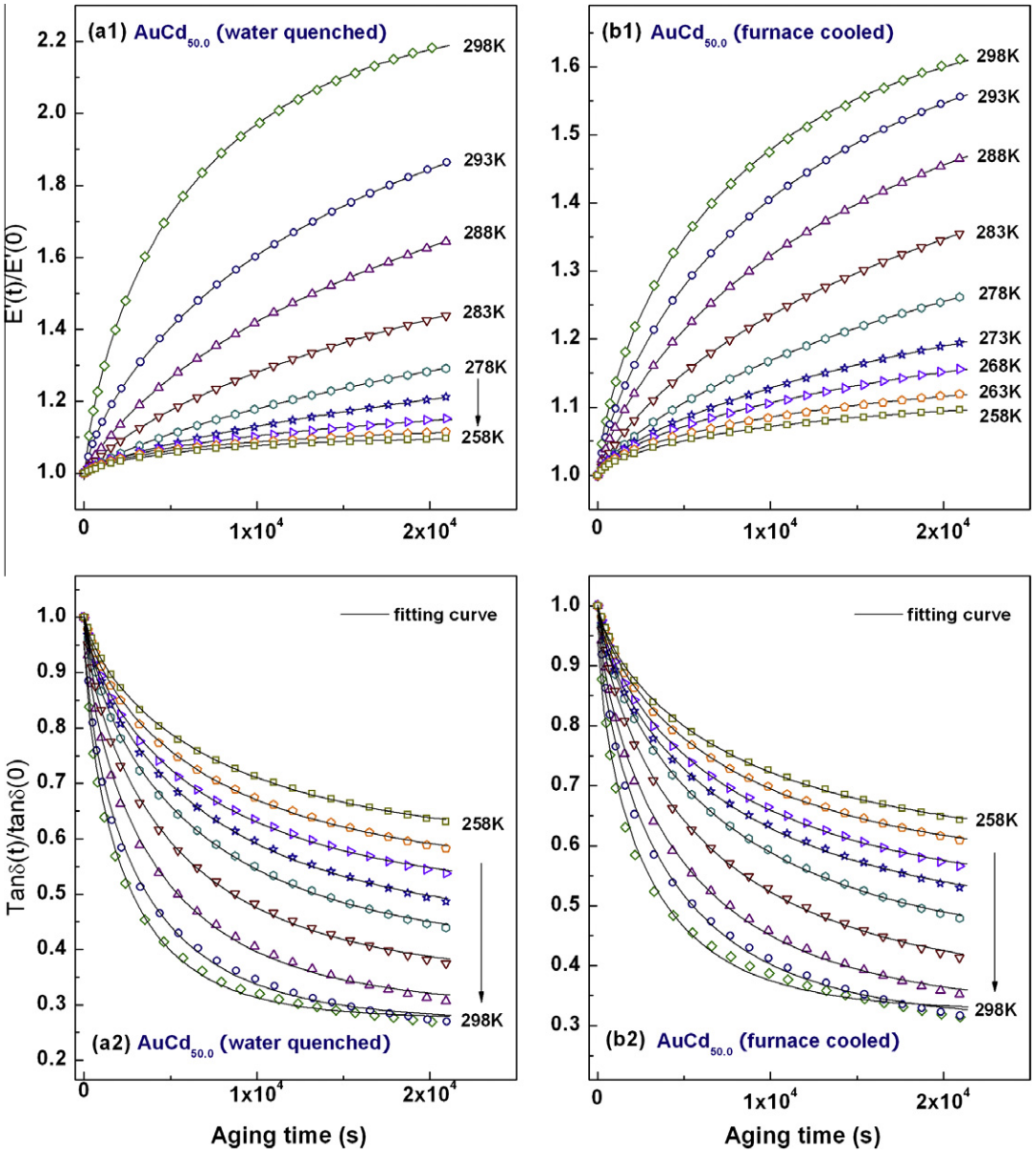

Fig. 7. Dots: evolution of storage modulus (a1 and a2) and internal friction (b1 and b2) of the water-quenched and furnace-cooled $AuCd_{50.0}$ alloy at different temperatures from 258 to 298 K, respectively; solid line: corresponding fitting curves by the stretched function.

natural to consider whether such dynamic properties changes during aging can also be explained by the same mechanism. Then, it is possible to unify the explanation for martensite aging effects on both static and dynamic properties. In the following, we will show that the evolution of storage modulus and internal friction during aging indeed can be understood based on the SC-SRO principle.

For simplicity, here we consider only two-dimensional (2-D) structures, but the argument is applicable to any three-dimensional (3-D) structures because only the symmetry is of relevance here. In order to illustrate easily, we suppose the structure of produced martensite phase is of tetragonal symmetry, although that of the Au–Cd alloys in this study is trigonal. It is well known that martensitic alloy undergoes a diffusionless symmetry-lowering transformation. The high temperature parent phase is of high symmetry (square lattice), the point defect symmetry is also cubic according to the SC-SRO principle (Fig. 9a). On cooling, the crystal symmetry changes to tetragonal abruptly at M_s (Fig. 9b). During this diffusionless process, the defect symmetry remains unchanged, because the change of defect symmetry requires the reconfiguration of point defects through diffusion. Thus, the fresh martensite of tetragonal crystal symmetry is embedded with point defects with cubic symmetry (Fig. 9b). According to the SC-SRO principle, this state is not stable and an equilibrium state is more favored, where the defect symmetry conforms to the tetragonal crystal symmetry. This gives rise to the martensite aging. With increasing aging time, the defect symmetry gradually follows the crystal symmetry through

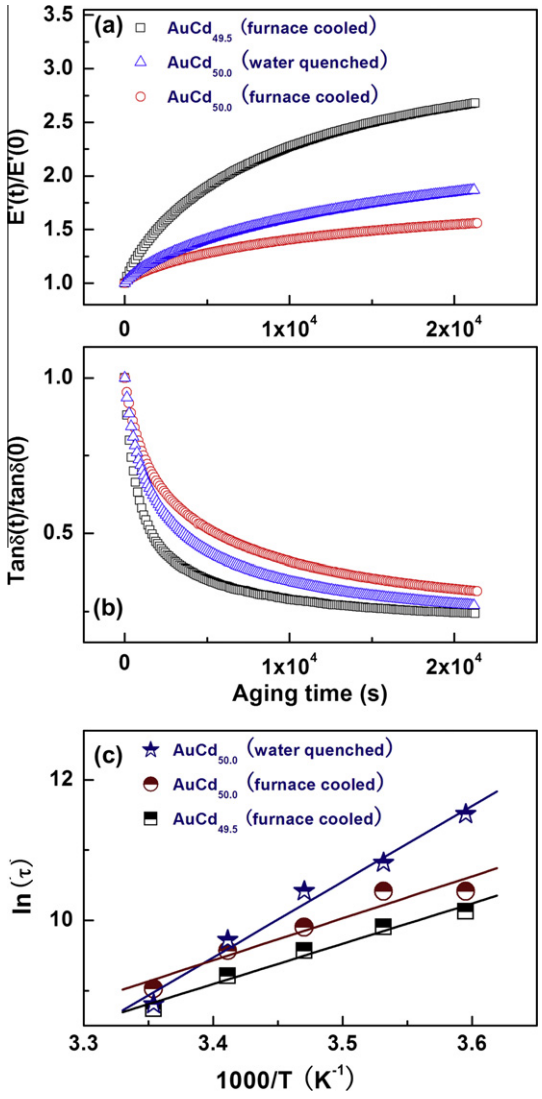

Fig. 8. Comparison of evolution of storage modulus (a) and internal friction (b) with aging time at 293 K, and the obtained relaxation time vs. aging temperature (c) between furnace-cooled $AuCd_{49.5}$ alloy, furnace-cooled and water-quenched $AuCd_{50.0}$ alloys.

the short-range migration of point defects and finally the defect symmetry becomes tetragonal in its stable state (Fig. 9c). Intuitively, we can consider this in the following way: with martensite aging, an internal stress field is gradually formed accompanying the gradual conforming of defect symmetry to the crystal symmetry and it is just this internal stress field that makes the aged martensite phase more stable than the fresh one. Such an idea was borrowed from the physically paralleled ferroic system, ferroelectrics, where an internal bias electric field was considered to exist after aging according to the same SC-SRO principle [34,35].

4.1.2. Understanding of the increase of storage modulus and decrease of internal friction with aging time

As is known, the static properties like the critical stress for the rearrangement of martensite variants correspond to a large-scale domain switching under external stress field, while the dynamic properties like the storage modulus or internal friction correspond to the intrinsic martensite phase deformation and twin boundaries motion under a small ac stress field. Previous studies have proved that the increase of critical stress after martensite aging is due to martensite domain stabilization, which makes the large-scale twin boundaries motion become more difficult. Similarly, the local twin boundaries motions are also restricted because of the martensite stabilization during aging, which gives rise to the increase of storage modulus and decrease of internal friction.

The standard definition of storage modulus shows that it is proportional to the small linear strain change caused by a small stress field. For multi-domain martensitic alloys, the strain is composed of two parts. One is from the intrinsic elastic deformation of martensite phase; the other is from the twin boundaries motion under external stress. Therefore, the storage modulus can be described by the following equation:

$$E' = \frac{\Delta\sigma}{\Delta\varepsilon_{IN} + \Delta\varepsilon_{TB}} \tag{3}$$

where E' is the storage modulus, $\Delta\sigma$ is the change of external stress, $\Delta\varepsilon_{IN}$ is the strain change from the intrinsic elastic deformation of martensite phase and $\Delta\varepsilon_{TB}$ is the strain change from the twin boundaries motion. As stated above, martensite aging mainly restricts the motion of twin boundaries, thus only the influence of aging on $\Delta\varepsilon_{TB}$ is considered. For the internal friction in the martensite state, it is mainly due to the hysteretic twin boundaries motion under ac stress field, so the value of internal friction is proportional to the twin boundaries mobility [28,36]. The higher twin boundaries mobility gives rise to larger internal friction.

Then the question is the origin of immobility of twin boundaries during martensite aging. Two possibilities are considered here. One is the short-range order change within the bulk martensite. The other is the pinning of twin boundaries by defects [17,18,37].

In Fig. 10, we schematically explain the evolution of storage modulus and internal friction by the former mechanism, i.e. the SC-SRO principle. Before aging, the defect symmetry of the fresh martensite is cubic and it has no restriction to the twin boundaries motion. Therefore, the twin boundaries can response freely to the external stress field, which induces a fairly large change of strain ($\Delta\varepsilon_{TB}$) and the corresponding storage modulus is small according to Eq. (3). At the same time, the internal friction associated with the hysteretic twin boundaries motion is large. By contrast, after aging, according to the SC-SRO principle, the defect symmetry conforms to the crystal symmetry in each martensite domain and stabilizes the domain configuration. Thus, when the external stress field is applied, the twin boundaries motion becomes more difficult, because any change of strain will encounter a resistance from the defect configuration which stabilizes their original orientation. As

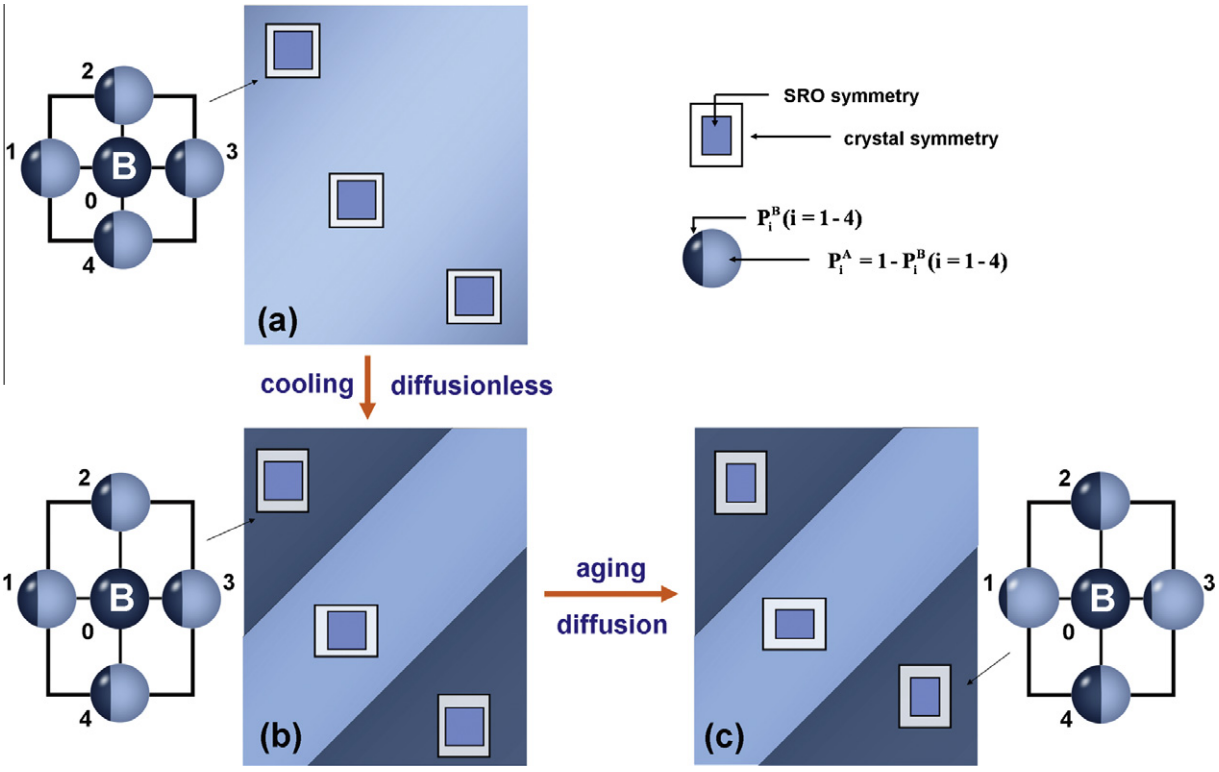

Fig. 9. Schematic illustration for the martensitic transformation and the following aging process according to the SC-SRO mechanism: (a) fresh parent phase, (b) fresh martensite phase, and (c) aged martensite phase. P_i^B (or P_i^A) is the conditional probability of defect B (or an atom A) occupying site i ($i = 1$, 2, 3, 4) if a defect B is at site 0. The values of P_i^B and P_i^A are represented by dark and light areas, respectively. They are uniquely related to SRO parameters.

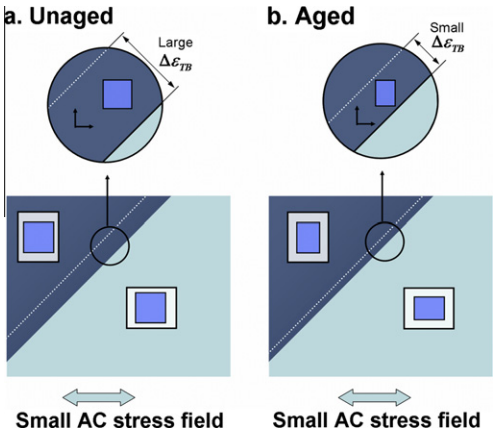

Fig. 10. Schematic illustration for the twin boundaries motion under ac stress field for (a) unaged martensite phase and (b) aged martensite phase. $\Delta\varepsilon_{TB}$ represents the strain change induced by twin boundaries motion.

a result, $\Delta\varepsilon_{TB}$ decreases after aging, and the corresponding storage modulus becomes larger. Meanwhile, as the mobility of twin boundaries is decreased, the associated internal friction is also decreased. As the short-range migration of point defects gradually occurs during the aging process, the $\Delta\varepsilon_{TB}$ also gradually decreases with increasing aging time. As a consequence, we observed the gradual increase of storage modulus and gradual decrease of internal friction with aging time.

For the twin boundary pinning mechanism, it allows the long-range diffusion of defects (such as vacancies) into twin boundaries, thus immobilizing them [17,18,37]. As a result, $\Delta\varepsilon_{TB}$ gradually decreases and consequently the storage modulus increases with aging. Meanwhile, the associated internal friction also becomes small. The long-range migration of point defects to twin boundaries gives rise to the gradual time-dependent change. In order to clarify whether the bulk effect or the twin boundary pinning effect contributes to the martensite aging on dynamic properties dominantly, further critical investigation on the single domain martensite is still required.

Nevertheless, the activation energy obtained in the present study seems to support the short-range migration of point defects during martensite aging, which favors the bulk mechanism involving short-range ordering of point defects. For long-range diffusion, the activation energy will be given as a summation of the migration energy (E_m) and the formation energy (E_f) of a vacancy [4,33,38]. For short-range diffusion, it is usually assisted by the migration of existing vacancies in the material, thus the activation energy is only the migration energy (E_m) [4]. It is reported that the activation energy for long-range diffusion in $AuCd_{49.0}$ alloy is $E_m + E_f = 0.95$ eV [4,38], which is much larger than that of martensite aging obtained for $AuCd_{49.5}$ (0.46 eV in the present study and 0.44 eV by Murakami et al. [4]) Meanwhile, the activation energy for long-range diffusion in $AuCd_{50.0}$ is $E_m + E_f = 1.22$ eV [4,33]. The value of martensite aging is 0.49 eV for furnace-cooled $AuCd_{50.0}$ and is 0.84 eV for water-quenched $AuCd_{50.0}$. They are also

much smaller than the above value for long-range diffusion. The comparison indicates that the diffusion of point defects during martensite aging may favor short range rather than long range. Such low activation energy is also responsible for the fact that the aging proceeds by a short time, even at room temperature.

It should be noted that a similar evolution of dynamic properties has been reported in aged ferroelectrics, i.e. the dielectric compliance (inverse of dielectric permittivity) increases and dielectric loss decreases with aging time [39,40], and such behaviors were also schematically understood in a similar way as shown in Fig. 10 [39].

4.1.3. Understanding of the temperature dependence

As discussed in the previous subsection, the evolution of dynamic properties results from the domain stabilization involving the short-range diffusion of point defects. When aging at high temperatures, the diffusion of point defects is fast, and the conforming of defect symmetry to the crystal symmetry can be finished in a short time. Thus, the relaxation time of high-temperature aging is short, as seen in Fig. 4a, and the evolution of dynamic properties is fast. On the contrary, when aging at low temperatures, the diffusion of point defects is slow and the conforming of defect symmetry to the crystal symmetry requires a comparatively longer time. Thus, the relaxation time of low-temperature aging is much longer; this is consistent with the results shown in Fig. 4a, i.e. the lower the aging temperature, the longer the relaxation time.

Furthermore, it is easy to see in Fig. 3 that, at the same aging time, the change of dynamic properties increases with increasing aging temperature. Such behavior can also be seen in the static properties during martensite aging, for instance, the increased value of critical stress is larger when aging at higher temperature [4]. These results indicate the martensite aging is a thermally activated process. However, the origin of temperature dependence of the relative change is still unclear. We think it may be understood by considering that different amount of point defects are involved in atomic reconfiguration at different aging temperatures. But further investigation is still required for a coherent and clear understanding.

4.1.4. Understanding of the point defect concentration dependence

The comparison of three aged alloys with different defect concentration in Fig. 8 shows that the changes of dynamic properties during martensite aging become more pronounced with increasing defect concentration. Such strong defect concentration dependence can be understood by considering the fact that the martensite aging is characterized by the defect diffusion process driven by the SC-SRO principle. When the defect concentration is large, more defects are involved in diffusion process so that the defect symmetry follows the crystal symmetry. Thus the martensite phase is stabilized by more defects after aging, and the change of strain and twin boundary motion will encounter a larger resistance from the defect configuration. As a result, the increase of storage modulus and decrease of internal friction will be more pronounced. With decreasing defect concentration, fewer point defects are involved in the diffusion process. Therefore, the corresponding change of storage modulus and internal friction also becomes less pronounced.

4.2. Modeling

4.2.1. Role of internal stress field on the evolution of free energy of martensite phase during aging

In the following, we attempt to give a theoretical description for the aging effects on the dynamic properties phenomenologically by introducing a time-dependent variable coupled with the order parameter to a Landau-type model. Such a time-dependent variable corresponds to the rearrangement process of point defects. Just as mentioned in the above subsection, the martensite aging process can be viewed as a process where an internal stress field is established gradually to stabilize the martensite phase. Such an internal stress field can be considered as the stress induced by elastic straining of the crystal lattice when the defects configuration conforms to the symmetry of crystal by diffusion [23]. Thus, the dynamic properties are affected with the existence of such an internal stress field.

It is helpful to envision the martensitic transformation as a distortion of the parent phase structure into martensite structure. Then one can construct the free energy of the system as a function of order parameter. A generic form of Landau free energy that can reproduce first-order martensitic transformation is a polynomial of the form

$$F(\eta, T) = \frac{1}{2}a(T - T_0)\eta^2 + \frac{1}{4}b\eta^4 + \frac{1}{6}c\eta^6 \tag{4}$$

where η is the order parameter, i.e. the characteristic lattice distortion; a (positive), b (negative) and c (positive) are coefficients [2], T is the temperature and T_0 is the lowest temperature at which martensite phase could exist as a metastable phase. An internal stress field σ_{in} coupled to the order parameter η contributes to the free energy by $-\sigma_{in}\eta$. In this case the total free energy is given by

$$F(\eta, T) = \frac{1}{2}a(T - T_0)\eta^2 + \frac{1}{4}b\eta^4 + \frac{1}{6}c\eta^6 - \sigma_{in}\eta \tag{5}$$

The expression is our thermodynamic model for describing the free energy of aged martensite. Thus, in order to see the evolution of free energy during aging, one should firstly determine the time-dependence of the internal stress field σ_{in}. In the simplest approach the time variation of the internal stress field σ_{in} may be considered linearly related to the derivatives of the Gibbs free energy, i.e. $\tau\frac{\partial\sigma_{in}}{\partial t} = -\kappa\frac{\partial F(\eta,T)}{\partial\eta}$ [23]. The equation must be resolved with the boundary conditions $\sigma_{in}(0) = 0$ and $\sigma_{in}(\infty) = \sigma^{\infty}$ as aging is considered to correspond to the building up of the internal stress field σ_{in}. Thus the time-dependence of the internal stress field σ_{in} is expressed as

$$\sigma_{in} = \sigma^{\infty}[1 - \exp(-t/\tau)] \quad (6)$$

Based on Eq. (6), a schematic curve describing the evolution of this internal field with aging time is shown in Fig. 11a. We selected four states with different internal stress field during the aging process, indicated by filled circles 1, 2, 3, 4 in Fig 11a. Fig. 11b schematically shows the free energy as a function of the order parameter η corresponding to these four states during the aging process. Immediately after cooling down to the martensite phase, the minimum of the free energy curve is at a non-zero order parameter, corresponding to the state without aging, indicated by filled circle 1. However, the defect symmetry remains cubic just after the martensitic transformation, producing an unstable situation where the non-cubic martensite phase is embedded with cubic defect symmetry. Thus there is a thermodynamic driving force to change the defect symmetry into the crystal symmetry where the free energy is lower according to the SC-SRO mechanism. As a result, martensite aging involving the defect reconfiguration takes place and the free energy decreases gradually with increasing internal field σ_{in}, as indicated by filled circles 2, 3. When the defect symmetry is the same as the crystal symmetry, as indicated by filled circle 4, the free energy is the lowest and the aged martensite phase reaches its thermodynamic equilibrium state.

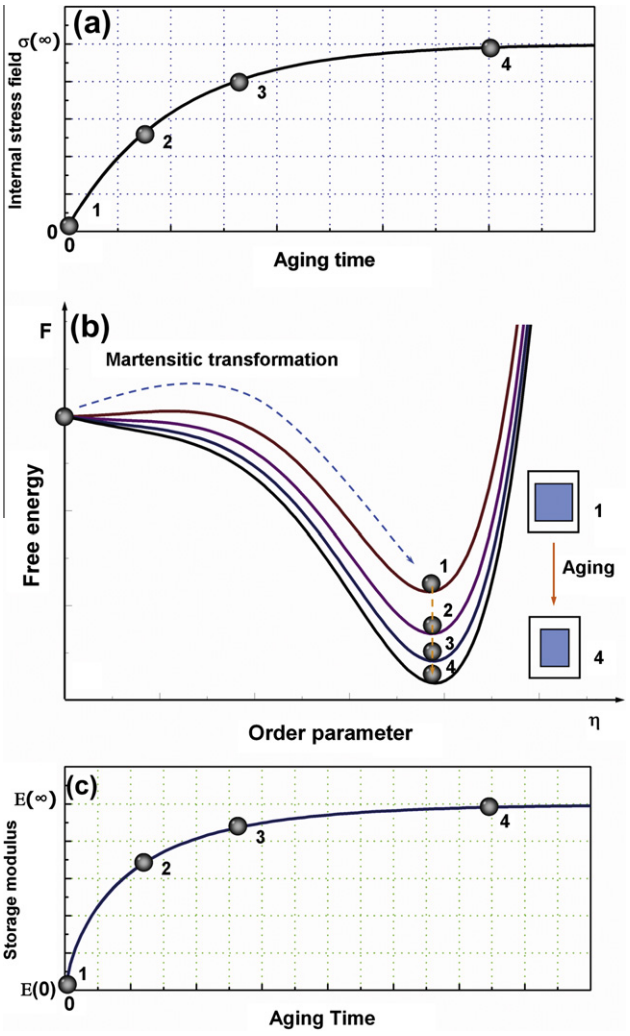

Fig. 11. Schematic illustration for the evolution of internal stress field (a), the corresponding change of free energy (b) and storage modulus (c) during martensite aging. (1) Represents the state before aging; (2 and 3) represent the intermediate states during aging; (4) represents the final state of aging, where the martensite phase is in equilibrium state.

4.2.2. The increase of storage modulus as a result of the building up of the internal stress field

In this subsection, we will show how the storage modulus evolves with aging time based on the internal stress field expressed in Eq. (6). The equilibrium of an isothermal system is given by the minimization of the free energy F (Eq. (5)) with respect to the order parameter, i.e. $\frac{\partial F(\eta,T)}{\partial \eta} = 0$, thus

$$a(T - T_0)\eta + b\eta^3 + c\eta^5 - \sigma_{in} = 0 \quad (7)$$

At the transformation temperature, the parent phase and the martensite phase has the same free energy, i.e. $F(\eta, T)_P = F(\eta, T)_M$, thus

$$\frac{1}{2}a(T - T_0)\eta^2 + \frac{1}{4}b\eta^4 + \frac{1}{6}c\eta^6 - \sigma_{in}\eta = 0 \quad (8)$$

Combining Eqs. (7) and (8), the order parameter of the martensite phase is given by

$$\eta = \eta_0 + \delta\sigma_{in} \quad (9)$$

where η is the order parameter of martensite phase; η_0, equal to $\sqrt{-\frac{3b}{4c}}$, is the order parameter of the fresh martensite before aging. The $\delta\sigma_{in}$ is the fraction of order parameter induced by the internal stress field σ_{in}, where $\delta = -\frac{4c}{3b^2}$. It should be noted here that we ignore the temperature dependence of the order parameter of martensite phase for simplicity and for real cases the order parameter of martensite increases slightly with decreasing temperature.

On the other hand, the storage modulus of the system is the second derivative of the free energy:

$$E' = \frac{\partial^2 F(\eta, T)}{\partial \eta^2} = a(T - T_0) + 3b\eta^2 + 5c\eta^4 \quad (10)$$

Combining Eqs. (9) and (10), the internal stress field σ_{in} can be introduced into the storage modulus E'. As the term $\delta\sigma_{in}$ in Eq. (9) is small compared to the order parameter of martensite phase, the storage modulus could be obtained approximatively by utilizing the first-order Taylor expansion, which reads

$$\begin{aligned} E' &= a(T - T_0) + 3b\eta_0^2 + 5c\eta_0^4 + 6b\eta_0\delta\sigma_{in} + 20c\eta_0^3\delta\sigma_{in} \\ &= E'_0 + \delta'\sigma_{in} \end{aligned} \quad (11)$$

where E'_0 is the storage modulus before aging and δ' is a measure of influence of the internal stress field σ_{in} on the storage modulus, which is equal to $6\sqrt{\frac{-3c}{b}}$. From this function we can easily see that the larger the internal bias field is, the larger the storage modulus becomes, as the coefficient δ' is positive. Therefore, with the increase of the internal stress field during martensite aging, the storage modulus will gradually increase. Then the storage modulus change with aging time can be obtained from Eqs. (6) and (11):

$$E' = E'_0 + \delta'\sigma^{\infty}[1 - \exp(-t/\tau)] \quad (12)$$

Eq. (12) has the same form as Eq. (1), which indicates our modeling is consistent with our experimental data. The schematic illustration for the evolution of storage modulus with aging time according to Eq. (12) is shown in Fig. 11c. The circled 1, 2, 3, 4 correspond to the four states indicated in Fig. 11a and b. It should be noted that in Eq. (12) the internal stress field σ_{in} is considered to be built up by a classic Debye relaxation; but for the real case the situation would be complex, thus an exponent β is introduced to the stretched exponential equation (Eq. (1)).

By introducing a time-dependent internal stress field into the Landau-type free-energy model, the evolution of free energy and dynamic properties during martensite aging process can be described. This suggests that the martensite aging can be viewed as a process where an internal stress field is built up gradually through the gradual reconfiguration of point defects and this internal stress seems to play the same role as that of the secondary slow variable proposed by other researchers [21–23].

5. Conclusions

On the one hand, we performed systematic experiments on Au–Cd shape memory alloys to probe the in situ change of dynamic properties, i.e. storage modulus and internal friction during the martensite aging process. On the other hand, we proposed a homogenous Landau-type model to characterize the change of storage modulus during martensite aging by introducing a time-dependent slow variable coupled with the order parameter. The main results and conclusions are drawn as follows.

(1) During martensite aging, the storage modulus shows a gradual increase while the internal friction shows a gradual decrease with increasing aging time.
(2) The evolution of dynamic properties with aging time obeys a simple relaxation function with activation energy of 0.46 eV for furnace-cooled $AuCd_{49.5}$ alloy. This value is consistent with reported one (~0.44 eV) obtained by research on the static properties during aging.
(3) The evolution of both storage modulus and internal friction shows strong dependence on the defect concentration of alloys and also on the temperature/frequency/displacement amplitude during dynamic loading.
(4) We suggest that all the observed characteristics of dynamic properties can be understood by the gradual stabilization of martensite phase during aging through the short-range reconfiguration of point defects, driven by the symmetry-conforming short-range order (SC-SRO) principle. In addition, the twin boundary pinning may also be a possible contribution to the observed aging effects.
(5) The evolution of storage modulus during martensite aging can be modeled phenomenologically by introducing a time-dependent internal stress field to the homogenous Landau-type potential and the obtained results are consistent with our experimental observations.

Acknowledgements

The authors gratefully acknowledge the support of National Natural Science Foundation of China (Grants Nos. 50720145101 and 50771079), National Basic Research Program of China (Grant No. 2010CB631003), as well as NCET and 111 project of China (B06025).

References

[1] Otsuka K, Wayman CM, editors. Shape memory materials. Cambridge: Cambridge University Press; 1998.
[2] Salje EKH. Phase transitions in ferroelastic and co-elastic crystals. Cambridge: Cambridge University Press; 1990.
[3] Ölander A. J Am Chem Soc 1932;54:3819.
[4] Murakami Y, Nakajima Y, Otsuka K, Ohba T, Matsuo R, Ohshima K. Mater Sci Eng A 1997;237:87.
[5] Miura S, Maeda S, Nakanishi N. Philos Mag 1974;30:565.
[6] Arab AA, Ahlers M. Acta Metall 1988;36:2627.
[7] Barceló G, Rapacioli R, Ahlers M. Scripta Metall 1978;12:1069.
[8] Sakamoto H, Otsuka K, Shimizu K. Scripta Metall 1977;11:607.
[9] Santamarta R, Seguí C, Pons J, Cesari E. Scripta Mater 1999;41:867.
[10] Seguí C, Cesari E, Font J, Muntasell J, Chernenko VA. Scripta Mater 2005;53:315.
[11] Miyazaki S, Otsuka K. In: Funakubo H, editor. Shape memory alloys. New York: Gordon and Breach; 1987. p. 116.
[12] Ren X, Otsuka K. Nature 1997;389:579.
[13] Otsuka K, Ren X. Scripta Mater 2004;50:207.
[14] Ren X, Otsuka K. Phys Rev Lett 2000;85:1016.
[15] Zangwill A, Bruinsma R. Phys Rev Lett 1984;53:1073.
[16] Marukawa K, Tsuchiya K. Scripta Metall 1995;32:77.
[17] Birnbaum HK, Read TA. Trans AIME 1960;218:662.
[18] Nakanishi N, Mori T, Miura S, Murakami Y, Kachi S. Philos Mag 1973;28:277.
[19] Otsuka K, Ren X. Phase Trans 1999;69:329.
[20] Ren XB, Otsuka K. MRS Bull 2002;27:115.
[21] Ohta T. Mater Sci Eng A 2001;312:57.
[22] Okuzono T, Yamazaki Y, Ohta T. Phys Rev B 2003;67:054106.
[23] L'vov VA, Kosogor A, Soderberg O, Hannula S-P. Mater Sci Forum 2010;635:13.
[24] Deng J, Ding X, Lookman T, Suzuki T, Otsuka K, Sun J, et al. Phys Rev B 2010;81:220101.
[25] Zhou Y, Fan G, Xue D, Ding X, Otsuka K, Sun J, et al. Scripta Mater 2009;61:805.
[26] Inamura T, Yamamoto Y, Hosoda H, Kim HY, Miyazaki S. Acta Mater 2010;58:2535.
[27] Mazzolai FM, Biscarini A, Coluzzi B, Mazzolai G, Villa E, Tuissi A. Acta Mater 2007;55:4243.
[28] Fan G, Zhou Y, Otsuka K, Ren X, Nakamura K, Ohba T, et al. Acta Mater 2006;54:5221.
[29] Murakami Y, Otsuka K, Mizubayashi H, Suzuki T. In: Proc int conf on displacive phase transformations and their applications in materials engineering. New York: TMS; 1998. p. 225.
[30] Hessinger J, Knorr K. Phys Rev B 1993;47:14813.
[31] Signorini GF, Barrat J-L, Klein ML. J Chem Phys 1990;92:1294.

[32] Chung SH, Stevens JR. Am J Phys 1991;59:1024.
[33] Gupta D, Lazarus D, Lieberman DS. Phys Rev 1967;153:863.
[34] Xue D, Gao J, Zhang L, Bao H, Liu W, Zhou C, et al. Appl Phys Lett 2009;94:082902.
[35] Bao H, Xue D, Wang Y, Gao J, Zhang L, Yadav K, Ren X, Yang S, J Appl Phys 2011; in press.
[36] Coluzzi B, Biscarini A, Campanella R, Trotta L, Mazzolai G, Tuissi A, et al. Acta Mater 1999;47:1965.
[37] Miura S, Hashimoto S, Nakanishi N. Scripta Metall 1985;19:353.
[38] Wechsler MS. Acta Metall 1957;5:150.
[39] Zhang L, Ren X. Phys Rev B 2006;73:094121.
[40] Carl K, Hardtl KH. Ferroelectrics 1978;17:473.